Real-Time Modeling of Vascular Flow for Angiography Simulation

Xunlei Wu[1,2], Jérémie Allard[2], and Stéphane Cotin[1,3]

[1] Harvard Medical School, Boston, USA
`wu.xunlei@mgh.harvard.edu`
[2] SimGroup, CIMIT, Cambridge, USA
`jeremie.allard@codrt.fr`
[3] Alcove Project, LIFL/INRIA Futurs, Lille, France
`stephane.cotin@lifl.fr`

Abstract. Interventional neuroradiology is a growing field of minimally invasive therapies that includes embolization of aneurysms and arteriovenous malformations, carotid angioplasty and carotid stenting, and acute stroke therapy. Treatment is performed using image-guided instrument navigation through the patient's vasculature and requires intricate combination of visual and tactile coordination. In this paper we present a series of techniques for real-time high-fidelity simulation of angiographic studies. We focus in particular on the computation and visualization of blood flow and blood pressure distribution patterns, mixing of blood and contrast agent, and high-fidelity simulation of fluoroscopic images.

1 Introduction

Vascular diseases are the number one cause of death worldwide, with cardiovascular disease alone claiming an estimated 17.5 million deaths in 2005 [1]. An increasingly promising therapy for treating vascular diseases is interventional radiology procedures, where a guidewire-catheter combination is advanced under fluoroscopic guidance through the arterial system, thus allowing a minimally invasive therapy while reducing recovery time for the patient when compared to corresponding surgical procedures. However, the main difficulty in these therapies is navigating through the intricate human vascular system while relying on two-dimensional X-ray views of the patient. Yet, the best training method so far has been actual patients with a vascular pathology.

To reduce the risks due to training on patients, we have developed a real-time high-fidelity interventional neuroradiology simulator for physician training and procedure planning. The system relies on accurate patient-specific anatomical representations of the vascular anatomy [2] and uses new algorithms for fluoroscopic rendering and physics-based modeling of catheter-vessel interactions. The full body vascular model used in our simulator consists of over $4,000$ arterial and venous vessels, and is optimized for real-time collision detection and visualization of angiograms.

In this paper, we aim to improve the vascular flow modeling accuracy over existing approaches [3,4] and yet maintain a real-time performance in order to
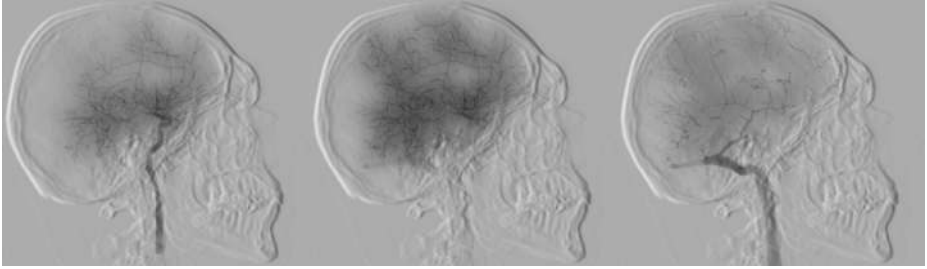
Fig. 1. High-fidelity real-time simulation of angiography in the brain, featuring contrast injection in arterial flow (*Left*); blush (*Middle*); and transition to venous side (*Right*)

improve training/planning immersiveness. We propose to simulate physiologic representations of arterial, parenchymal and venous phases of thoracic, cervical and intracranial vasculature. Synthetic fluoroscopy uses a volumetric approach which directly incorporates the same patient CT dataset as that used to reconstruct the vascular model. Laminar blood flow is modeled through a simplified version of the Navier-Stokes equations while contrast agent propagation is controlled by an advection-diffusion equation. The proposed method can handle very large anatomical dataset in real-time, and angiographic studies performed on our simulator closely approximate those on actual patients. This high level of fidelity is key to permit realistic simulation based training, and ultimately enables the planning and rehearsal of complex cases.

2 Real-Time Flow Computation in Large Vascular Networks

An angiogram is used to locate narrowing, occlusions, and other vascular abnormalities. By visualizing and measuring flow distributions in the vicinity of a lesion, angiographic studies play a vital role in the assessment of the pre- and post-operative physiological states of the patient. In this section we detail our real-time flow model, one of the three key elements of angiography simulation.

2.1 Flow Model

Aside from ventriculograms and some aortic angiograms, turbulent flow is rarely observed in interventional radiology procedures. In addition, flow distribution in the network is more relevant when identifying and quantifying vessel pathology than local fluid dynamic pattern. Hence, 1D laminar flow model is adequate under our application context.

Blood flow in each vessel is modeled as an incompressible viscous fluid flowing through a cylindrical pipe, and can be calculated from the Navier-Stokes equation. The resulting equation, called Poiseuille Law,

$$Q = \frac{\Delta P}{R} \quad with \quad R = \frac{8\eta L}{\pi r^4} \tag{1}$$

relates the vessel flow rate Q to the pressure drop ΔP, blood viscosity η, vessel radius r, and vessel length L. To compute such vascular flow, a set of algebraic equations are developed as follows. The arterial vasculature can be represented as a directed graph, with M edges and N nodes. If $M \neq N$, we form an augmented square matrix $\mathbf{K}$ by adding trivial equations, i.e. $\mathbf{P_s} = \mathbf{P_s}$ or $\mathbf{Q_s} = \mathbf{Q_s}$, to the set of Poiseuille equations. If $M < N$,

$$
\mathbf{Q} = \mathbf{KP} \quad or \quad
\begin{bmatrix} \vdots \\ Q_i \\ \vdots \\ \hline \mathbf{P_s} \end{bmatrix}
=
\begin{bmatrix} \vdots & \vdots & \vdots & \vdots & \vdots \\ 0 & \Omega_i & 0 & -\Omega_i & 0 \\ \vdots & \vdots & \vdots & \vdots & \vdots \\ \hline 0 \cdots & & \cdots & 0 & \mathbf{I} \end{bmatrix}
\begin{bmatrix} \vdots \\ P_j \\ \vdots \\ P_k \\ \vdots \end{bmatrix}
\tag{2}
$$

where $\Omega_i = 1/R_i$ is the vessel i flow resistance. Boundary conditions are then added to the system as Lagrange Multipliers. There are two groups of constraints. The first set corresponds to the prescribed pressure values at the beginning and end nodes of the directed graph. These pressure values are defined as a function of time, the depth of the node, and ventricular pressure. The deeper an end node is in the graph, its pressure value is smaller and less variant in time. The second set of constraints relates to the conservation of flow, similar to Kirchhoff's circuit laws in electric circuits, such that for any internal node, the total flow flowing toward this node is equal to the total flow flowing away from this node. This is described by $0 \equiv \sum Q_{in} + \sum Q_{out} = \Psi^T \mathbf{P}$. The final system matrix of our 1D flow model is

$$
\overline{\mathbf{Q}} \equiv \begin{bmatrix} \mathbf{Q} \\ \mathbf{P_e} \\ \mathbf{0} \end{bmatrix} = \overline{\mathbf{KP}} = \begin{bmatrix} \mathbf{K} & \Gamma & \Psi \\ \hline \Gamma^T & 0 & 0 \\ \Psi^T & 0 & 0 \end{bmatrix} \begin{bmatrix} \mathbf{P} \\ \lambda_\mathbf{e} \\ \lambda_\mathbf{f} \end{bmatrix}
\tag{3}
$$

where $\lambda_\mathbf{e}$ and $\lambda_\mathbf{f}$ are vectors of Lagrange multipliers, and where Γ is a permutation matrix. Each row of Ψ^T is a summation of multiple rows from the first M rows of $\mathbf{K}$ in (2). $\mathbf{P_e}$ is the vector contains prescribed nodal pressure value.

Because the prescribed pressures $\mathbf{P_e}$ are varying in time, $\overline{\mathbf{Q}} = [\cdots 0 \cdots P_e^T 0]^T$ (containing both the initial conditions $\mathbf{Q} = 0$ and boundary conditions) needs to be updated at the beginning of each time step. So that $\overline{\mathbf{P}} = \overline{\mathbf{K}}^{-1}\overline{\mathbf{Q}}$. As a subset of $\overline{\mathbf{Q}}$, $\mathbf{Q} = [\mathbf{K} \, \Gamma \, \Psi]\overline{\mathbf{P}}$. Our model assumes that the vascular resistance is invariant in time, so that $\overline{\mathbf{K}}^{-1}$ can be precomputed. This permits real-time computation rates, even on very large vascular models. It costs 50 milliseconds to compute the flow distribution for an arterial vasculature with $2,337$ vessels on an Athlon 64 X2 2.4GHz processor.

2.2 Modeling Local Blood Flow Alterations

For the purpose of training, it is important to have access to a variety of scenarios. Each scenario does not necessarily need to be based on an existing patient dataset, but could be derived from a generic dataset that is altered to resemble a specific pathology. Our simulation system permits the creation of a stenosis or aneurysm at any location, as well as automatically accounting for the change in blood flow that it effects.
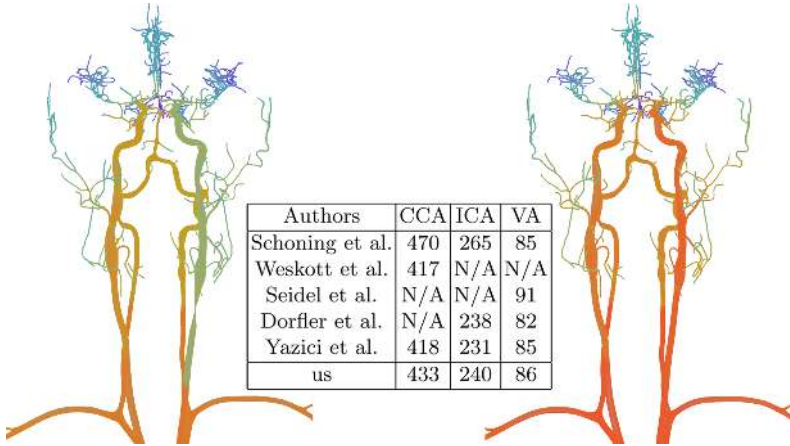
Authors	CCA	ICA	VA
Schoning et al.	470	265	85
Weskott et al.	417	N/A	N/A
Seidel et al.	N/A	N/A	91
Dorfler et al.	N/A	238	82
Yazici et al.	418	231	85
us	433	240	86

Fig. 2. *Left:* Blood pressure distribution due to a stenosis in the common carotid artery (CCA). *Right:* Restored blood pressure distribution after treatment. *Center:* Comparison of our computed blood flow (ml/min) in the CCA, internal carotid artery (ICA), and vertebral artery (VA) against the mean values measured by other authors [5].

Stenosis. During stenting or angioplasty simulation, a stent or balloon is deployed to expand the narrowed section of a vessel due to stenosis (as illustrated in the left of Figure 2). Therefore, the radius of the vessel is changed locally and its resistance is modified according to Equation (1). Assuming vessel i contains the stenosis, its initial resistance $R_i = R_1 + R_2 + R_s$ becomes $R_i' = R_i + (R_s' - R_s)$ after expanding the vessel's radius. This change in resistance requires $\overline{\mathbf{K}}$ to be updated as $\overline{\mathbf{K}}'$ as well as its inverse of $\overline{\mathbf{K}}'$. To maintain the simulation interactivity, the computation of $\overline{\mathbf{K}}'^{-1}$ needs to be done in real-time. Notice that the local changes in $\overline{\mathbf{K}}$, namely row i in $\overline{\mathbf{K}}$ and two rows in Ψ^T, can be rewritten as $\overline{\mathbf{K}}' = \overline{\mathbf{K}} + \mathbf{U}\mathbf{V}^T$, where vector $\mathbf{U}^T = \begin{bmatrix} \cdots 1 \cdots 1 \cdots -1 \cdots \end{bmatrix}$, vector $\mathbf{V}^T = \begin{bmatrix} \cdots \Delta\Omega_i \cdots -\Delta\Omega_i \cdots \end{bmatrix}$, and $\Delta\Omega_i = R_s' - R_s$ represents the weight change of vessel i two nodes. Given $\overline{\mathbf{K}}^{-1}$, $\overline{\mathbf{K}}'^{-1}$ can be efficiently computed using Woodbury's formula [1].

The added fluid during injecting contrast agent, in particular, also changes the flow rate around the tip of catheter. In our vascular flow model, such influence is modeled as the whole vessel's flowrate being modulated by the injection rate. To correctly model the change of flow distribution due to injection, $\overline{\mathbf{K}}$ is augmented with one additional boundary condition $Q_{inj} = (P_{i,0} - P_{i,1})/R_i = \begin{bmatrix} \cdots \Omega_i \cdots -\Omega_i \cdots \end{bmatrix} \overline{\mathbf{P}} = \mathbf{U_{inj}}^T \overline{\mathbf{P}}$ such that

$$\overline{\mathbf{K}}_{\mathbf{inj}} = \left[\begin{array}{c|c} \overline{\mathbf{K}} & \mathbf{U_{inj}} \\ \hline \mathbf{U_{inj}}^T & 0 \end{array} \right] \tag{4}$$

---

[1] http://mathworld.wolfram.com/WoodburyFormula.html

To achieve real-time performance, $\overline{\mathbf{K}}_{\mathbf{inj}}^{-1}$ must be computed efficiently as well. Given $\overline{\mathbf{K}}^{-1}$, this objective is achieved by using block matrix decomposition [2].

3   Contrast Agent Propagation

3.1   Advection-Diffusion Model

An angiogram is done by taking a continuous series of X-rays while injecting a contrast agent into the vascular structure under examination. The contrast agent, usually an iodine solution, provides the density needed for detailed X-ray study of the blood vessels. Upon injection, the contrast agent is carried by blood stream and circulates through the vascular system (arterial, and venous) until it is eliminated in the kidneys and liver. We model the transportation of contrast agent by an advection-diffusion equation describing the distribution of contrast agent concentrations $\mathbf{C}(x, d, t)$ as a function of curvilinear coordinates $\mathbf{x}$ along the centerline of a vessel, the distance $\mathbf{d}$ to the centerline, and time $\mathbf{t}$,

$$\frac{\partial C(x,d,t)}{\partial t} + u(x,d,t)\frac{\partial C(x,d,t)}{\partial x} + \kappa_C \nabla \cdot \nabla C(x,d,t) = I(x,t) \qquad (5)$$

where $I(x, t)$ is the injection rate of contrast agent, κ_C is the contrast agent diffusion factor and $u(x, d, t)$ is the laminar flow velocity along the axial direction of each vessel. From the vessel flow rate Q as computed by the vascular flow model (section 2), this velocity can be modeled as a parabolic profile:

$$u(x, d, t) = \frac{1}{4\eta}\frac{\Delta P}{\Delta x}(r^2 - d^2) = \frac{2}{\pi r^2}Q(1 - \frac{d^2}{r^2}) \qquad (6)$$

Compared to only modeling concentration at the centerline, as in most previous works, this model provides two important flow features: the propagation front profile is not flat, and some contrast agent remains longer in vessels due to the low velocity near the borders. Since a precise variation depending on the radial position is not visually important, interpolation between the value at the border and at the center is sufficient, using the square of the radial distance to maintain a parabolic profile. We also apply the following simplifications:

- At the center due to high velocity, the advection term is stronger than the diffusion, which can be neglected. We solve this advection numerically using a unconditionally-stable semi-implicit scheme [6].
- At the border, only the diffusion is relevant as the velocity is zero. This diffusion can be computed numerically by combining the value from the previous timestep with the concentration at the center.

The resulting contrast propagation is visible in Figure 1.

3.2   Visualization

In this section we describe various techniques used for rendering a simulated angiogram with a high level of fidelity. While prior work [7] as well as commercial

---

[2] http://sepwww.stanford.edu/public/docs/sep121/paper_html/node93.html

products rely on polygon-based rendering techniques to simulate X-ray images, we propose a method based on volume rendering. Such a technique can provide a high level of realism yet can be optimized for real-time rendering on current consumer GPU, such as the NVIDIA GeForce 8800 GTX in our system.

Simulated fluoroscopy. Fluoroscopy is an imaging modality that uses a *continuous* beam of X-rays visualize the patient's internal anatomy. It follows the same principle as X-ray imaging, where the attenuation of a X-ray beam depends on the density and thickness of the tissue it traverses. The attenuation of an X-ray beam traversing a thin slice of homogeneous material is given as

$$I = I_0 e^{-\mu d} \approx I_0 e^{-\sum_j \mu_j d_j} \tag{7}$$

with I_0 the initial intensity, μ the attenuation coefficient of the material, and d the traversed material thickness. In order to simulate accurately the fluoroscopic process, we have developed a volume rendering approach which renders a CT scan dataset using a discrete transfer function to approximate the continuous beam attenuation equation (7), where d_j corresponds to the slice thickness along the ray and μ_j is the sampled attenuation coefficient of the anatomic structure at slice i. The value of μ_j can be derived from the intensity of each voxel in the CT scan. By computing the contribution of each slice of the CT scan image to the decrease of energy of the X-ray beam, then by summing all the contributions, we can derive a realistic synthetic X-ray image. Since the voxel intensity is directly related to Hounsfield Units, μ can be determined from Hounsfield Units [7]. Similarly, slice thickness and intra-slice distance of the CT scan allows us to measure d_j. What remains to be computed are $e^{-\mu_i d_i}$ and the sum of the contribution over each slice. A good approximation of (7) can be implemented in OpenGL by blending a texture element with the corresponding frame buffer element, taking advantage of recent programmable graphics boards.

Multi-scale voxel representation. Our contrast agent propagation model is based on 1D advection-diffusion as discussed in Section 3.1. To visualize the angiogram in 3D, our previous work [7] created a volumetric representation of the vessels' lumen by dividing this interior space into equal sized voxel elements which are then associated with a curvilinear location x along each vessel. The contrast agent concentration value of a sample point along a vessel is then mapped to the voxels in their vicinity. To deal with very detailed vascular models where the vessels radii vary from $0.5mm$ to $17mm$, more than 40 million equal sized voxels with size $0.25 \times 0.25 \times 0.25mm^3$ was generated, which can no longer be rendered in real-time.

To maintain both high-resolution visualization and real-time rendering, we developed a multi-scale approach based on subdivision. Similar to marching-cube, starting from a prescribed initial grid size, each voxel is tested and labelled as *internal*, *boundary*, and *external*. While the internal voxels are stored, the boundary voxels are subdivided into 8 equal sized sub-voxels. Each sub-voxel is examined against the set of surface polygons intersected by the parent voxel. If

a sub-voxel does not intersect with surface and it is inside the surface, then that sub-voxel is labelled as internal and stored. Boundary sub-voxels are again subdivided. The iterative step continues until the predefined number of subdivisions is reached. As a result, starting from $2 \times 2 \times 2mm^3$ and 4 subdivision steps, i.e. the smallest particle is of $0.25 \times 0.25 \times 0.25mm^3$, we generate only 9.2 million multi-scale voxels.

Different sized particles have different amount of radiation attenuation under fluoroscopy. This is achieved by adjusting each particle's rendering size linearly and its intensity exponentially according to its dimensions. This approach is implemented using a programmable shader and runs at interactive frame rates.

Blush. As contrast agent propagates into invisible capillary vessels, it produces a blush that must be simulated, since it is an important visual cue for physicians. Unfortunately computing a volume-based diffusion would be time-prohibitive, so we instead use the GPU to compute an image-space diffusion. When the contrast agent propagates to small vessels in the blush area, we first render the multiscale particles, then use a two-pass (horizontal and vertical) convolution shader to compute a gaussian blur. The blur radius is tuned to achieve a high-level visual coherence with real angiogram. This image is then combined with the particles and x-ray volume to produces the final picture. The result, as shown in Figure 1, reproduces the visual effect with only a small impact on performance.

Cardiac and respiratory motion. Reproducing internal motions, mainly heart beating and respiratory motion, is required to produces realistic sequences. However, it is not possible to store and interactively render 4D scans, or animate by hand the vascular surface model. Instead, we rely on simple spatial affine transformations defined over a local volume of influence. Given a point p in 3D space, we compute its displaced position p' as follow :

$$p' = p + \sum_i smoothstep \left(\frac{1-|(p-center_i)/radius_i|}{1-core_i} \right) (M_i - I)p$$
$$smoothstep(x) = 0 \text{ if } x < 0, \quad 1 \text{ if } x > 1, \quad 3x^2 - 2x^3 \text{ otherwise}$$

(8)

where the volume of influence is defined by $center_i$, $radius_i$ and $core_i$, while the motion is defined by a 4×4 matrix M_i. This transformation is animated over time using a cyclic profile curve. Equation 8 is simple enough to be implemented inside vertex shaders on the GPU, enabling real-time deformations of both surface and volumetric objects. Moreover, all parameters can be edited interactively using a simple visual editor, as visible in Figure 3. It provides enough controls to create simple but realistic motions. One important limitation is that it does not distinguish between bones and tissues, which are equally deformed. However, we can fine-tune visually the influence of each motion, so that the cardiac motions does not move the nearby ribs, while the respiratory motion do.

4   Results

We have applied our methods to different datasets, and performed both qualitative and quantitative validations. Blood flow and blood pressure distributions
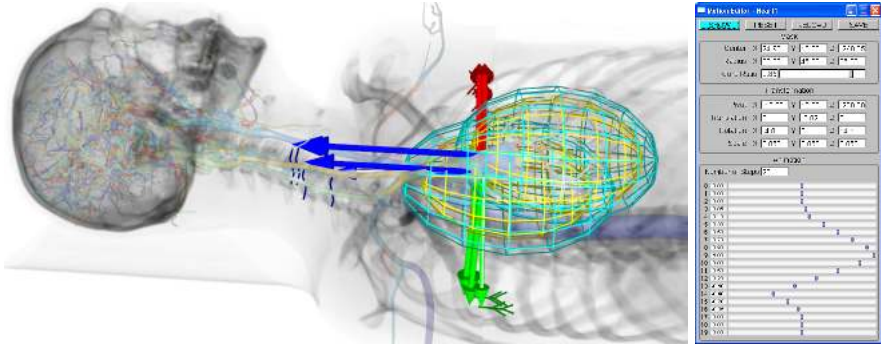
Fig. 3. *Left:* X-Ray rendering under deformation. *Right:* Interactive motion editor.

were computed on a dataset containing about 500 arterial vessels representing the cerebrovascular system, and on a dataset containing about 4,000 vessels (both arteries and veins) describing the full vascular circulation system with a higher level of detail in the brain. For both datasets the results were compared to results from Yazici *et al.* [5] as well as other studies referenced in [5]. The table in the center of Figure 2 compares various flow values in different main vessels of the cerebrovascular network. Our results match very closely these values, yet are computed in real-time. Changes in local flow patterns due to the treatment of a stenosis are also illustrated in the right of Figure 2. These results, as well as the real-time angiogram illustrated in Figure 1 are very similar to what can be observed during an actual procedure, and were qualitatively validated by a neuro-interventional radiologist.

5   Conclusion

We have proposed a series of methods for computing and rendering high-fidelity angiographic studies in real-time. These techniques can bring a new level of realism to simulation systems for interventional radiology, and increase the acceptance of such systems by the medical community.

References

1. Mackay, J., Mensah, G.: Atlas of Heart Disease and Stroke (2004)
2. Luboz, V., Wu, X., Krissian, K., Westin, C., Kikinis, R., Cotin, S., Dawson, S.: A segmentation and reconstruction technique for 3D vascular structures. In: Duncan, J.S., Gerig, G. (eds.) MICCAI 2005. LNCS, vol. 3749, pp. 43–50. Springer, Heidelberg (2005)
3. Alderliesten, T.: Simulation of Minimally-Invasive Vascular Interventions for Training Purposes. PhD dissertation, Utrecht University (2004)

4. Dawson, S., Cotin, S., Meglan, D., Shaffer, D., Ferrell, M.: Designing a computer-based simulator for interventional cardiology training. Catheterization and Cardiovascular Intervention 51(4), 522–527 (2000)
5. Yazici, B., Erdogmus, B., Tugay, A.: Cerebral blood flow measurements of the extracranial carotid and vertebral arteries with doppler ultrasonography in healthy adults. J. Diag. Interv. Radiol. 11, 195–198 (2005)
6. Stam, J.: Stable fluids. In: Proceedings of ACM SIGGRAPH 1999, pp. 121–128 (1999)
7. Manivannan, M., Cotin, S., Srinivasan, M., Dawson, S.: Real-time pc-based x-ray simulation for interventional radiology training. In: Proc. MMVR, pp. 233–239 (2003)